Identification of novel microcephaly-linked protein ABBA that mediates cortical progenitor cell division and corticogenesis through NEDD9-RhoA

Aurelie Carabalona[1], Henna Kallo[2], Liliia Andriichuk[2], Maryanne Gonzalez[2], Ellinoora Elomaa[3,4], Florence Molinari[5], Christiana Fragkou[1], Pekka Lappalainen[6], Marja Wessels[7], Juha Saarikangas[2,3,4], Claudio Rivera[1,2]

1 Aix Marseille Univ, INSERM, INMED, Marseille, France
2 Neuroscience Center, HiLIFE, University of Helsinki, Helsinki, Finland
3 Helsinki Institute of Life Science, HiLIFE
4 Faculty of Biological and Environmental Sciences, University of Helsinki, Helsinki, Finland
5 Aix Marseille Univ, Inserm, MMG, Marseille, France
6 Institute of Biotechnology, HiLIFE, University of Helsinki, Helsinki, Finland.
7 Department of Clinical Genetics, Erasmus MC, University Medical Center Rotterdam, Rotterdam, The Netherlands.

Corresponding Author: Aurelie.carabalona@inserm.fr and Claudio.rivera@helsinki.fi

Abstract

The cerebral cortex is responsible for higher cognitive functions. Its correct development depends on coordinated asymmetric division cycles by polarized radial glial progenitor cells. Mitotic defects in neuronal stem cells are linked to the aetiology of microcephaly, but the underlying mechanisms remain incompletely understood. Here we describe a novel role of the membrane deforming cytoskeletal regulator protein Abba (MTSS1L/MTSS2) in cortical development. Loss of Abba in the developing brain resulted in radial glia proliferation arrest, disorganized radial fibers and abnormal migration of neuronal progenitors. During cell division, Abba localized to the cleavage furrow where it recruited the scaffolding protein Nedd9 and positively regulated RhoA activity. Importantly, we identified a human variant Abba (R671W) in a patient with microcephaly and intellectual disability. Ectopic expression of this mutant protein in mice phenocopied Abba knockdown. Taken together, these data provide novel mechanistic insight into human microcephaly and cortical development by identifying ABBA as a novel regulator of faithful mitotic progression of neuronal progenitor cells.

Introduction

Development of the central nervous system occurs by proliferation of neural progenitor cells, migration and differentiation of their progeny over substantial distance. These different steps require extensive membrane remodelling and cytoskeleton dynamics[1]. Neuronal migration involves the coordinated extension and adhesion of the leading process along the radial glial scaffold with the forward translocation of the nucleus, which requires regulation of centrosome and microtubule dynamics by different proteins[1–3]. However, little is known about the molecular mechanisms underlying membrane dynamics during neuronal migration and morphogenesis.

Cell membrane curvature is a micro morphological change involved in many important cellular processes including endocytosis, exocytosis, and migration[4]. Recent studies demonstrated that the members of an extended protein family, characterized by the presence of a membrane binding and deforming BAR (Bin–Amphiphysin–Rvs) domain function at the interface between the actin cytoskeleton and plasma membrane during the formation of membrane protrusions or invaginations[5–7]. These proteins have been shown to be important for proper neuronal morphogenesis[8], and can either generate positive membrane curvature to facilitate the formation of plasma membrane invaginations (e.g. BAR, N-BAR and F-BAR domain proteins) or induce negative membrane curvature to promote the formation of plasma membrane protrusions (I-BAR and IF-BAR domain proteins)[9,10]. An important part of the membrane deforming mechanism include the interaction with phosphatidylinositol-4,5-biphosphate (PI(4,5)P2)-rich membranes through their BAR domain and also with actin cytoskeleton through Wasp Homology-2 domain (WH2).

Regulation of the actin cytoskeleton plays a crucial role in several developmentally important cellular processes including neuronal migration, axonal and dendritic extension and guidance, and dendritic spines formation[11]. We previously discovered that MIM, a member of the I-BAR protein family, has an important role in bending the dendritic plasma membrane in order to form dendritic spines and sculpt their morphology[12]. In a more recent study, a closely related protein Abba (MTSS1L) was found to be important for exercise induced increase synaptic potentiation in the hippocampus[13]. Although an important role of MIM and Abba in synapse formation and plasticity starts to emerge, information about the role of the early expression of this protein family during development is poor.

Mutations in BAR domain proteins are increasingly found in mental retardation disorders. For instance, altered expression and mutation of F-BAR family proteins, SrGAP2 & 3, are known to be associated to neurological disorders (mental retardation, the 3p syndrome, schizophrenia, early infantile epileptic encephalopathy and severe psychomotor delay[14–18]). Furthermore, previous whole-exome sequencing of pre-screened multiplex consanguineous families identified ABBA as a likely candidate linked

to neurogenic disorders[19], suggesting that some BAR containing proteins might play important functions during brain development. Despite Abba's potential role in neuronal development, very little is known about how this protein may lead to neurological pathology.

Regulation of the actin cytoskeleton and plasma membrane dynamics in glial cells of the developing brain has remained poorly understood. Interestingly, the I-BAR protein Abba is the only glia-enriched regulator that has been reported so far[20].

We sought to determine the consequences of altered expression of *Abba* in radial glial progenitor (RGP) cells on cell cycle progression and neurogenesis and to test for subsequent neuronal migration. To address these issues, we used *in utero* electroporation to silence *ABBA* with shRNA in embryonic mouse brains. Downregulation of Abba's expression had a striking effect on RGP cells progression, resulting in a blocking of cytokinesis and a subsequent apoptosis. Biochemical analysis demonstrated that the cytokinesis block was due to an absence of interaction with the adhesion docking protein named Nedd9 (aka CAS-L or HEF1) that is well known to be a positive regulator of RhoA signaling in mitosis[21]. Using FRET based monitoring of RhoA activity we also found a significant role of Abba on RhoA activity. Moreover, we observed a defect in neuronal migration associated with an increase in neuronal apoptosis. Importantly, we identified 1 patient harboring different mutations in *ABBA* sequence and sharing similar features such as: small head circumference, mental retardation, autism spectrum disorder (ASD) and craniofacial dysmorphism. We provide evidence that the (2011C>T(R671W)) patient mutation likely represents a dominant loss-of-function allele.

Overall, our data highlights the critical role of *Abba* in proper cortical development in neurogenesis and migration, and provides the first evidence that *ABBA* is a new causative gene for cortical malformation associated with ASD.

Materials and Methods

Plasmids construction

We used one shRNA targeting the coding sequence for Abba[20], Nedd9 shRNA was designed using the siRNA Wizard Software (InvivoGen ©), as negative control we used a non-targeting shRNA. These shRNAs were subcloned into an mU6pro vector[22], and co-injected with a pCAG-RFP vector to visualize fluorescent cells. Abba mouse full length with silent mutations[20], ABBA human full length and the dominant negative construct ABBA-R671W human were made by GeneCust© (France) and subcloned into the pCAGIG-IRES-GFP vector (Addgene, Cambridge, MA, USA).

Bioinformatic methods

Abba coding sequences were obtained from NCBI. The multiple sequence comparison was done by Log-Expectation (MUSCLE) method and visualized with DNASTAR MegAlign Pro. The impact of Abba R671W on the structure and function of a human Abba protein was predicted using PolyPhen-2 and HumVar model[23].

Human subjects

Families were identified through our clinical and research programs, personal communication, as well as the MatchMaker Exchange (MME) including GeneMatcher[24] (http://www.genematcher.org). Informed consent for publication and analysis of photos, imaging and clinical data was obtained from the patients' legal guardians. Brain magnetic resonance imaging (MRI) studies were performed on the subject and reviewed by the investigators in accordance with Department Ethical permission number (MEC-2012387) to conduct human exome studies.

RhoA activity assay

Fluorescence from Raichu-Rac1 was imaged using a confocal microscope (LSM 710/Axio; Carl Zeiss) controlled by ZEN 2011 software (Carl Zeiss) and equipped with water immersion objective (63×/1.0 NA; Carl Zeiss). Transfected cells were illuminated with an argon laser (Lasos; Lasertechnik GmbH) at 458 nm (CFP and FRET) and 514 nm (YFP) using 0.5–10% of full laser power. Emission was collected at 461–519 nm (CFP) and 519–621 nm (FRET and YFP). The pinhole was fully opened. Scanning was performed in XY mode using 6× digital zoom that resulted in a pixel XY size of 68 × 68 nm. FRET signal was calculated as reported elsewhere[23]. In brief, using ImageJ 1.48v software images where background subtracted and FRET image generated using three images: MDonor (CFP excitation and CFP emission filters), MIndirectAcceptor (CFP excitation and YFP emission filters), and MDirectAcceptor (YFP excitation and YFP emission filters), using the following equation: $FRET = (MIndirectAcceptor - MDonor \times \beta - MDirectAcceptor \times (\gamma - \alpha\beta))/(1 - \beta\delta)$. Coefficients α, β, δ, and γ were obtained by independent control experiments analyzing cells expressing CFP or YFP as described previously[25]. Coefficients α, δ, and γ were determined in cells expressing only YFP (acceptor) and calculated according to equations: $\alpha = MDonor/MDirectAcceptor$; $\gamma = MIndirectAcceptor/MDirectAcceptor$; $\delta = MDonor/MIndirectAcceptor$. Coefficient β was determined in cells expressing only CFP (donor) and calculated according to the equation: $\beta = MIndirectAcceptor/MDonor$. After generation of FRET image, intensity of FRET signal was calculated using a mask obtained from a corresponding YFP image and covering neuronal cell bodies.

In Utero Electroporation

Animal experiments were performed in agreement with European directive 2010/63/UE and received approval N°: APAFIS#2797 from the French Ministry for Research and in agreement with the National Animal Experiment Board, Finland (license number ESAVI/18276/2018).Plasmids were transfected using intraventricular injection followed by *in utero* electroporation[26,27]. Timed pregnant C57BL6N mice (Janvier Labs; E14; E0 was defined as the day of confirmation of sperm-positive vaginal plug) received buprenorphine (Buprecare,0.03 mg/kg) and were anesthetized with sevoflurane/isoflurane (4%-4.5% induction, 2% -anaesthesia maintenance) 30 minutes later. For pain management, bupivacaine (2 mg/kg) was administered via a subcutaneous injection at the site of the future incision. Uterine horns were exposed, the lateral ventricle of each embryo was injected using pulled glass capillaries and a microinjector (Picospritzer II; General Valve Corporation, Fairfield, NJ, USA) with Fast Green (2 mg/ml; Sigma, St Louis, MO, USA) combined with the different DNA constructs at 1.5 µg/µl or with 1.5 µg/µl shRNA constructs together with 0.5 µg/µl pCAGGS-RFP. Plasmids were further electroporated by discharging a 4000 mF capacitor charged to 50V with a BTX ECM 830 electroporator (BTX Harvard Apparatus, Holliston, MA, USA). The voltage was discharged in five electrical pulses at 950ms intervals via 5mm tweezer-type electrodes laterally pinching the head of each embryo through the uterus. The mice were followed-up post-surgically and given buprenorphine (Buprecare 0.03 mg/kg) if needed. The number of animals has been calculated on the basis of the requirement for adequate numbers of brain slices and sections for sufficient imaging to provide statistically significant data on the effects of RNAi, small molecules, and other reagents used in the proposed analysis, plus controls.

Organotypic cultures and Live Imaging

To assess the impact of altered ABBA expression in the RGP cells on neurogenesis and cell cycle progression, we utilized a combination of *in utero* electroporation and time-lapse imaging of organotypic cultures. The organotypic cultures were prepared as described[28] with the following exceptions. After surrounding the brains (E17) with 4.5% UltraPure Low Melting Point Agarose (Invitrogen, 16520-100), 350 µm thick slices were cut with Vibratome 1000 Plus Sectioning System (No. 054018). Before placing the slices on a coated (83 µg/ml Laminin, Sigma L2020; 8,3 µg/ml Poly-L-Lysine, Sigma P4707) cell culture insert (Millicell, PICMORG50), sections were carefully cleaned from agarose to ensure adequate oxygenation. The inserts with slice cultures were transferred into a 6-well plate containing 1 ml of warmed slice culture medium. For live-imaging we used Andor Dragonfly 550 high speed Spinning Disc confocal equipped with Nikon Perfect Focus System, motorized XY stage, and environmental chamber. The system uses Fusion 2.0 software (version 2.1.0.48). The image acquisition was

executed using Andor iXon 888 U3 EMCCD camera, 20x magnification with voxel size 0.65 x 0.65 x 0.9524 micron^3 (channel/excitation: RFP/561 nm, GFP/488 nm). Time lapse-imaging of organotypic cultures was started at E17+DIV0 with intervals of 10 minutes and total duration of 15 hours. The data was collected from 6 pups (2 scramble, 4 shRNA), 17 slices (5 scramble, 12 shRNA) and 24 areas (9 scramble, 15 shRNA; some slices were recorded from two different areas).

Immunostaining of Brain Slices

Mice brains were fixed (E17) in Antigen Fix (Diapath), Brain slices were sectioned coronally (80µm) on a vibratome (Leica microsystems). Brain slices were washed with PBS (Phosphate-buffered saline pH 7.4) and stained in PBS 0.3% Triton X-100 supplemented with 5% of donkey serum. Primary antibodies were incubated overnight at 4°C, sections were then washed with PBS and incubated in secondary antibodies for 2 hours at room temperature. Antibodies used in this study were: Abba (homemade), Vimentin (Millipore, MAB3400), KI67 (Millipore, AB9260), phospho-histone H3 (Abcam, ab14955), Pax6 (biolegend, PRB-278P).

Cells culture and transfection

Rat C6 glioma cells were cultured at 37°C under a humidified atmosphere with 5% CO2 with a complete medium DMEM supplemented with 10% foetal bovine serum (FBS, Sigma) and 100 units/mL antibiotics/antimycotics. Cells were transfected using the Neon® Transfection System (Life Technologies) according to the manufacturer's protocol. Briefly, cells were trypsinized and counted with the cell counter SCEPTER (Millipore). Electroporation was performed with 500 000 cells and a total amount of 5 µg of DNA containing a reporter plasmid encoding RFP (1:5) and shRNAs or mismatch constructs, with the following configuration: 1860 V, 1 pulse, 20 ms. Cells were then cultured on a 6 wells plate during 2 days before RNA extraction.

Immunocytochemistry

HEK293T cells were fixed in Antigen Fix (Diapath), for 15 min and blocked at room temperature for 1 h with 5% normal goat serum,0.3% Triton X-100 in PBS and incubated overnight at 4°C with a set of antibodies against Abba (homemade), Phalloidin (Thermo Fisher, A12379), Nedd9 (Abcam, ab18056), Hoechst (Thermo Fisher, 62249). Cells were then washed with PBS and incubated in secondary antibodies for 2 hours at room temperature.

RT-PCR and qPCR

Total RNA was isolated from C6 using RNeasy Plus Mini kit and cDNA was synthesized using the Quantitect Reverse Transcription kit, according to the manufacturer's protocol (QIAGEN). Quantitative PCR (qPCR) was performed on a Light cycler 480 using SYBR-

Green chemistry (Roche) and specific primers for Abba (F: CGAGACTCGCTGCAGTATTCC and R: CCATTCACAGAGTAGCAGTCG, 113 bp), Nedd9 (Qiagen, QT01610385) and CyclophilinA (Qiagen, QT00177394) as a control probe. qPCR was performed with 5 µL of diluted cDNA template, specific primers (0.6 µM) and SYBR Green I Master Mix (7.5 µL) at a final volume of 15 µL. Each reaction was performed at an annealing temperature of 60°C and for 50 cycles. Reactions were performed in duplicate and melting-curve analysis was performed to assess the specificity of each amplification. A standard curve was performed for each gene with a control cDNA diluted at different concentrations. Relative expression was assessed with the calculated concentration in respect to the standard. All experiments were performed in triplicate.

Microscopy and Image Analysis

All images were collected with an IX80 laser scanning confocal microscope (LSM 710/Axio; Carl Zeiss) controlled by ZEN 2011 software (Carl Zeiss)). Cells & Brain sections were imaged using a 60x 1.42 N.A. oil objective or a 10x 0.40 N.A. air objective. All images were analyzed using ImageJ (NIH, Bethesda, MD). To quantify the total number of C6 cells alive and in mitosis on 12mm diameter coverslips 2 & 3 days after Abba shRNA & control transfections, we have arbitrary designed 4 identical regions comprised of 9 squares using ZEN software acquisition system and count manually the total number of alive and mitotic cells in each condition.

Statistical data

Statistical analyses were performed with Prism (GraphPad Software, La Jolla, CA, USA). A two-sample Student's t-test was used to compare means of two independent groups if the distribution of the data was normal. If the values come from a Gaussian distribution (D'agostino-Pearson omnibus normality test) the parametric unpaired t-test with Welch's correction was used. But, when the normality test failed, the non-parametric Mann–Whitney test was used. Significance was accepted at the level of $p < 0.05$.

No statistical methods were used to predetermine sample sizes, but our sample sizes are similar to those generally employed in the field. No randomization was used to collect all the data, but they were quantified blindly.

Yeast two□hybrid screen

Yeast two□hybrid screening was performed by Hybrigenics Services (Paris, France). The Abba coding sequence containing amino acids (aa) 1□715 was cloned into pB27 (N-LexA-bait-C fusion) and pB66 (N-GAL4-bait-C fusion) and sequence verified. These constructs were used as baits to screen the mouse embryo brain RP2 prey library. Total of 91 million (pB27) and 31 (pB66) million interactions were analyzed and the detected

interactions were assigned with statistical confidence score, the Predicted Biological Score (PBS) (www.hybrigenics-services.com).

Co-immunoprecipitation

C6 cells were washed with ice cold PBS and lysed using lysis buffer (20 mM Tris-HCl [pH 8,0], 137 mM NaCl, 10% glycerol, 1% Triton X-100, 2 mM EDTA) with 50 µg/ml PMSF (Roche) and a protease inhibitor cocktail (Roche). Cell lysate was agitated for 30 min at 4°C and centrifuged at 12000 rpm for 20 min at 4°C. The supernatant was collected and protein concentrations were determined with a Pierce™ BCA Protein Assay kit, according to the manufacturer's protocol (Thermo Scientific).

Before Co-IP, lysates were precleared with washed Pierce Protein A/G Magnetic Beads (Thermo Scientific) overnight in gentle shaking at 4°C, to remove nonspecific binding. Beads used for Co-IP were washed and preblocked with 3% BSA in PBS overnight in gentle shaking at 4 °C. Washing steps were done using a wash buffer (1% BSA, 150 mM NaCl, 0,1% Tween-20 in TBS).

For Co-IP, 1000 µg of protein from precleared lysate was incubated with 20 µl of specific primary antibodies (Abba: homemade; Nedd9: Abcam, ab18056) overnight in gentle shaking at 4°C. Negative controls were incubated without primary antibodies under the same conditions. Immunocomplexes were pulled down by incubating the antigen-antibody mixture with preblocked beads for 1 h in gentle shaking at room temperature. Beads were washed 3 times with wash buffer and once with purified water before elution. Bound proteins were eluted from the beads by incubating them in 1 x Laemmli buffer containing 150 mM NaCl for 10 min at room temperature.

Original C6 cell lysate and immunoprecipitated proteins were resolved by SDS-PAGE (4-20% Mini-PROTEAN TGX Gel; Bio-Rad) and transferred using Trans-Blot Turbo Mini PVDF Transfer Packs and Transfer System (Bio-Rad). Membranes were blocked with TBS containing 0,1% Tween-20 and 5% milk and blotted with primary antibodies overnight in shaking at 4°C. HRP-conjugated secondary antibodies used in this study were Rabbit anti-mouse IgG and Goat anti-rabbit IgG (Invitrogen). Protein bands were visualized using the ChemiDoc™ MP imaging system (Bio-Rad).

Results

Abba knockdown disrupted radial glia morphology

Previous studies of the expression pattern of Abba in the developing brain has disclosed a conspicuous expression in radial glia. In order to investigate the function of

Abba in the developing brain, we used a mouse *in utero* RNAi approach to knockdown Abba at E14. For this purpose, we used shRNA knockdown using a previously validated targeting sequence[20]. Evaluation of knockdown efficiency in rat C6 glioma cells showed a 70–80% reduction of Abba mRNA and protein levels (Supplementary Figure 1).
To determine whether knockdown of Abba expression alters neuronal migration, Abba-shRNA3 combined with a red fluorescent protein (RFP) construct was introduced into neural proge nitor cells of mouse neocortex by *in utero* electroporation at E14 and evaluated at E16-18 (Figure 1A). Electroporation of E14 targets the progenitors that will migrate and populate cortical layers II/III neurons. In E17 brain sections, we observed that some neurons previously electroporated at 3 days earlier with the scrambled construct reached the cortical plate as expected (Figure 1B). However, *in utero* expression of Abba-shRNA3 induced a significant arrest of cells within the ventricular zone (VZ) (Figure 1A-C; scramble 24.3 ± 6.4%; n=9, Abba-shRNA3 63.7 ± 2.9%; <0.0001; n=8). Surprisingly, we also observed a striking decrease in the total number of RFP positive cells in brain sections electroporated with Abba-shRNA3 at E17 and E18 (Figure 1D-E; scramble 969.2±109.0 cells/mm^2; n=9, Abba-shRNA3 311.3±28.61 cells/mm^2; <0.0001; n=8). These results indicate an important role of Abba in the proliferation and migration of cortical neuronal progenitors.

We also evaluated the impact of Abba knockdown on radial glial morphology by imaging vimentin-stained Abba knockdown cells at 3 days post-electroporation. All E17 Abba knockdown brains, but not in age-matched controls, displayed disruption of radial glial fibers in the VZ/SVZ (Figure 1D and F). Control vimentin-positive cells displayed the characteristic features and polarized morphology of radial glia with processes extending from the VZ to the pial surface. In contrast, in Abba knockdown brains, vimentin-positive cells exhibited misoriented apical processes, detached end feet in the ventricular surface (Figure 1D) and decreased number of radial glial progenitor cells in the VZ (Figure 1F; scramble 126.5 ± 13.4cells, n=8; Abba-shRNA3 65.1 ± 26.2cells, n=7; p=0.0033). All together these data show that the loss of Abba can disrupt radial glial cells morphology thus affecting their progenitor function.

These data suggest that Abba is required for radial glial organization, neuronal migration, regulation of neuronal proliferation and cell survival. Importantly, these results are in accord with the reported association of Abba with developmental neurological diseases including intellectual disability and microcephaly[19]

ABBA is required for cell cycle progression of radial glia progenitors

Development of the cerebral cortex occurs through a series of stages, beginning with RGPs. These stem cells exhibit an unusual form of cell-cycle-dependent nuclear oscillation between the apical and the basal regions of the ventricular zone, known as

interkinetic nuclear migration (INM). RGP cells undergo mitosis only when they reach the SVZ[29,30]. It has been shown that inhibition of INM disrupts RGP cell cycle progression[31–33]. To test the effect of altered radial glial cell morphology on cell cycle progression, we have quantified the nuclear distance from the VS for RGP cells after electroporation of scrambled or Abba RNAi (Figure 2A). We observed an accumulation of Abba-shRNA RGP cells close to the ventricular surface (0-10 µm; scramble 30.2 ± 3.2%, n=7; Abba-shRNA3 38.3 ± 2.3%, n=7; p= 0,000156) which can correspond to mitotic cell, but also further away (>30 µm; scramble 12.0 ± 3.3%, n=7; Abba-shRNA3 21.9 ± 2.4%, n=7; p= 0,000023) which support our previous observations on cells detaching from the VS (Figure 1D and F). Furthermore, we observed that Abba ShRNA decrease the percentage of the RGP cells marker Pax6 (Figure 2B and C; scramble 31,9 ± 0,6%, n=8; Abba-shRNA3 21,1 ± 0,6%, n=5; p=<0.0001). We have then tested for cell cycle effects, and found a decrease on the percentage of Abba shRNA-expressing RGP cells positive for the cell cycle marker Ki67 (Figure 2D and E; scramble 46.5 ± 0,8%, n=7; Abba-shRNA3 23,7 ± 1,369%, n=5; p= <0.0001) and also for the late G2/M phases marker phospho-histone H3 (PH3, Figure 2F and G; scramble 4,5 ± 0,1764%, n=9; Abba-shRNA3 1,264 ± 0,5191%, n=5; p= <0.0001). These results strongly argue for a major role of Abba in cell cycle progression.

Abba localizes to the cleavage furrow and is important for cytokinesis

To characterize the specific role of Abba in mitotic progression, we synchronized C6 rat glioma cell line and stained with Abba antibody. We found that Abba localized to the putative apical membrane initiation site and cytokinetic bridge, proximal to the contractile actin ring during late telophase and cytokinesis (Figure 3A and B respectively). The actomyosin contractile ring is formed at the plasma membrane in response to accumulation of phosphoinositide 4,5 bisphosphate (PI(4,5)P2) to generate constricting force to separate the two daughter cells[34]. Abba is known to interact with PI(4,5)P2 via its membrane deforming I-BAR domain[20] that has the capacity to deform and recognise the membrane curvature.

To determine the impact of the loss of Abba on cytokinesis, we quantified the number of C6 cells in cytokinesis 3 days after transfection with Abba-shRNA or scramble shRNA. Importantly we found a two-and-a-half-fold increase in the percentage of Abba shRNA-expressing cells in cytokinesis (Figure 3B and D; scramble 0,8285 ± 0,1161%, n=12; Abba-shRNA 2,078 ± 0,2682%, n=12; p= 0,0358), suggesting a prominent role of Abba in cytokinesis. To validate this *in vivo*, we performed live imaging in cortical organotypic slices from animals that were *in utero* electroporated with either Abba-shRNA or scramble vectors. Analysis of live imaging recording showed a strong mitotic block at the ventricular surface (Figure 2C). We then examined the impact of cytokinesis block on cell survival and found a lower total number of cells 4 days after transfection with

Abba-shRNA3 compared with control scramble (Figure 3E; scramble 380,3 ± 48,16%, n=12; Abba-shRNA3 155,8 ± 22,32%, n=12; p= <0.0001). Taken together, these data provide evidence that Abba is required for completion of mitosis resulting in reduced number of progenies.

Abba recruits Nedd9 to the cytokinetic bridge and is required for RhoA activation

To decipher the mechanism by which Abba is involved in mitosis, we performed a yeast-two-hybrid (Y2H) screen in E10.5-E12.5 mouse brain embryo library using full length mouse Abba as a bait. The resulting analysis identified three high (PBS: B) / good (PBS: C) confidence interactors: the E3 ubiquitin ligase Beta-Trcp2 (PBS: B), scaffolding protein Nedd9 (PBS: C) and the transcription factor Otx2 (PBS: C) (Fig 4A). Among these candidate proteins, Nedd9 (aka HEF-1 or Cas-L) caught our interest as it was previously reported in breast cancer cells to localize to the cleavage furrow during cytokinesis where it activates RhoA, as well as abnormal expression of Nedd9 results in cytokinesis defect[21,35,36] (Figure 4B).

We first tested whether Abba and Nedd9 physically interact, as suggested by the Y2H screen. To this end, we performed immunoprecipitation experiments in C6 cells using anti-Nedd9 as well as anti-Abba antibodies. The precipitated Nedd9-Abba complex was separated on SDS-page and followed by western blot with anti-Abba and anti-Nedd9 antibodies respectively. Indeed, Abba precipitated with Nedd9 in both directions, but not using control beads (Figure 4C). We then analyzed whether interaction with Abba is important for Nedd9 stability by western blot which showed no decrease in Nedd9 expression upon Abba depletion (data not shown), indicating that Abba does not affect Nedd9 stability. Interestingly however, when we analyzed the localization of Nedd9, we found that Abba was required for targeting Nedd9 to the cleavage furrow/cytokinetic bridge (Figure 4D). These data suggest that Abba recruits Nedd9 to the cleavage furrow during RGP cells division, which fits to its role in sensing curved PI(4,5)P2 rich membranes. Nedd9 plays a role in RGP cytokinesis *in vivo*. To knockdown Nedd9, we used shRNA targeting Nedd9 which reduced mRNA levels by 75% in C6 cells (Supplementary Figure 2A). To determine whether knockdown of Nedd9 expression alters RGP cells morphology and function, Nedd9-shRNA combined with a red fluorescent protein (RFP) construct was introduced into neural progenitor cells of mouse neocortex by *in utero* electroporation at E14 and stained with the radial glial cells marker, vimentin. Interestingly, similarly to Abba knockdown, Nedd9 downregulation resulted in disruption of INM as a larger portion of progenitors accumulated close to the ventricular surface (Figure 4E-F; scramble 25 ± 2.30% n=8, Nedd9-shRNA 46.92±2.78%; n=7; p=<0.0001). Using the late G2/M phases marker, PH3, we observed similar results as with Abba shRNA and point mutation no difference

in number of PH3 positive cells (Supplementary figure 2C; scramble, 4.50 ± 0.18%, n = 9; Nedd9-shRNA, 5.07 ± 0.35%, n = 6, P = 0,1135). These data provide evidence that both Abba and Nedd9 function to ensure correct mitotic completion of RGP cells.

Finally, to determine whether Abba is important for Nedd9 activity and how Abba and Nedd9 converge to regulate the cell-cycle, we assessed the activity of RhoA, a downstream signalling molecule of Nedd9[37] which is important for cytokinetic actomyosin ring assembly and dynamics[37–39]. To determine RhoA activity we used a GFP-based FRET construct for RhoA designated ‘‘Ras and interacting protein chimeric unit’’ Raichu-RhoA in C6 cells. In order to test the efficacy of the assay we used Calpeptin, a RhoA activator which, as expected, increased RhoA activity (Raichu-RhoA without calpeptin: 12.15±0.36 n=52; Raichu-RhoA with Calpeptin: 14.48±0.61 n=33; p = 0.002) confirming the functionality of our assay (Figure 5A upper panel). Importantly, when Abba was silenced by shRNA there was a significant 34% decrease in Raichu-RhoA activity as compared to the control shRNA treated cells (Figure 5A lower panel and B; scramble 12.03±0.34; n=81, Abba-shRNA 7.93±0.34; n=27; p<0.0001). These data provide support for the function of Abba in spatial assembly of cytokinetic signaling through the Nedd9-RhoA axis.

Identification of ABBA missense variant R671W in an individual with neurodevelopmental syndrome

Mutations in genes effecting mitotic progression of neuronal progenitors have been linked to neurodevelopmental disorders[40]. Importantly, we identified a patient carrying a novel heterozygous missense variant in ABBA coding *MTSS1l/MTSS2* gene. This mutation (2011C>T(R671W)) affects residues that are conserved from Zebrafish to Human and reside in exon 15 (Figure 6A and B). Consistent with a de *novo* origin of the variant, it was not found in the parents of the affected individual or in normal controls. This patient presents some characteristic craniofacial dysmorphism as mild deep-set eyes, thickened helices, synophrys, narrow forehead, bitemporal narrowing, small bilateral epicanthal folds, upslanting palpebral fissures, medial flaring of eyebrows, flat midface, V-shaped palate, and dysmorphic ears. Brain magnetic resonance imaging sequences showed the presence of a microcephalic brain associated with a smaller head linked to mild IQ. The patient also suffered from Attention-Deficit/Hyperactivity Disorder *(*ADHD) (Figure 6C, Table 1). Moreover, through Gene matcher[24] website, we were able to identify two additional patients carrying the same ABBA variant that shared similar brain malformation (personal communication with Dr.G.Lemire and Dr.L.Briere).The variant replaces an arginine to tryptophan that has a large aromatic group that could lead to destabilization of a tertiary structure. Indeed, bioinformatic prediction using AlphaFold predicts (pLDDT) with high 84.4 confidence score that R671 is located in an alpha helical fold close to the C-terminal end of the protein[41]. Furthermore, analysis using Poly-Phen-2 structure and sequence-based algorithm to

predict the impact of R671W substitution on the structure and function of ABBA, we found a high probability that the mutation is damaging for the protein function[23] (Naïve bayes probability score 0.952) (Figure 6D).

Expression of R671W Human variant results in defects in mitosis and neuronal migration

To test the effects of the human missense variant in mouse brain development, we introduced the human ABBA cDNA encoding either wild type or patient mutation R671W into developing mouse brains by *in utero* electroporation at E14 followed by imaging and quantification of targeted cell at E17. Interestingly, whereas wild type ABBA (ABBA-FL) expression showed no defects in radial glial morphology or neuronal migration, the R671W mutant expression resulted in disorganized radial glial fibers and accumulation of multipolar neurons in the SVZ/lower IZ with very few bipolar neurons (Figure 6E). When analyzing the distribution of electroporated neuron progenitors, we observed clear accumulation in the VZ/SVZ (Figure 6F; ABBA-FL 18.67±1.44%; n=8, ABBA-R671W 39.77±2.73% n=6; P=0.0001). We also found a significant increase in RGP nuclei at the VS of the brain (Figure 6G, C ABBA-FL 32.56±2.58%; n=8, ABBA-R671W 50,04±2.04%; n =6; p=0.000001. Interestingly, no difference in accumulation of PH3+ cells was found (Supplementary Figure 2 B and C; Abba-human-WT 4.50 ± 0.17%; n=9, Abba-human-mutation 4.71 ± 1.98%; p=0.76; n=5), indicative of a dysfunction in neuronal maturation. These data show that ectopic expression of the R671W mutation, but not wild type protein, results in aberrant development of developing cortex. Taken together, these data provide evidence that the missense mutation in ABBA found in the patient could be linked to abnormal brain development.

Discussion

Abba was originally identified as a novel regulator of actin and plasma membrane dynamics specifically in radial glial C6 cells[20]. However, its role on brain RGP cells *in vivo* had remained unclear. In this study we found that reduced expression of Abba in radial glia of the cortical ventricular zone leads to impaired radial migration and radial glia organization. Most interesting Abba knock-down specifically blocked cytokinesis in radial glia progenitors (RGP) cells, resulting in abnormal RGP cells morphology, mitosis and decreased glial and neuronal numbers. The mechanism for this action appears to include impaired signaling through actin regulatory protein RhoA probably through the interaction with Nedd9 during early and late stages of telophase. Consistent with these results we found that a missense variant in a patient with microcephaly and intellectual disability in its clinical picture. Overexpression of the mutant protein in mice cortical progenitors resulted in phenotypes similar to cortical Abba down regulation indicating

that Abba and the mechanism disclosed in this study are relevant for normal human brain development.

Radial glial exiting from cytokinesis requires Abba

BAR proteins can interact with PI(4,5)P_2 -rich membranes through their BAR domain, and several studies indicate that PI(4,5)P_2 play a central role in cytokinesis. Indeed, it has been reported that in mammalian cells PI(4,5)P_2 accumulates at the cleavage furrow and recruits membrane proteins required for stability of the furrow because of a role in adhesion between the contractile ring and the plasma membrane. Moreover, overexpression of proteins that bind to PI(4,5)P_2 perturbs cytokinesis completion, by interfering with adhesion of the plasma membrane to the contractile ring at the furrow, but not ingression of the cleavage furrow[42,43]. Immunocytochemistry of Abba shows a strong accumulation at the cleavage furrow. In addition, in absence of Abba, we observed an accumulation of cells blocked in cytokinesis (Figure 3). these observations and previous findings showing that Abba can interact with PI(4,5)P_2 -rich membranes through its BAR domain as well as with the actin cytoskeleton through Wasp Homology-2 domain (WH2), lead us suspect that Abba could link the actin contractile ring to the plasma membrane and participate in the mechanism for the invagination of the nuclear membrane during cytokinesis.

Abba interacts with Nedd9 to regulate RhoA activity

Here we have found that Abba interacts directly with Nedd9 during cytokinesis and down regulation of Abba leads to significant changes in RhoA activation. Nedd9 is a focal adhesion protein involved in mitotic entry and cleavage furrow ingression[44]. Similar to the results found in this study, previous results have shown that cells with abnormal expression of Nedd9 remain in G1 subsequently leading to cell apoptosis[36]. This is consistent with the view that Nedd9 triggers cells to enter mitosis. Nedd9 is known to be a positive regulator of RhoA signaling in mitosis. Indeed, activation of RhoA is required for cell rounding at early stages of mitosis and cleavage furrow ingression, and deactivation of RhoA is essential for cell abscission[21]. Moreover, it has been shown that Nedd9 overexpression blocks cells at abscission by maintaining levels of RhoA activation, and decreased Nedd9 expression inhibits cleavage furrow ingression by non-activated RhoA pathway. In light of these results, we hypothesized that during cytokinesis at the cleavage furrow the membrane composition change and is enriched in PI(4,5)P_2 leading to Abba recruitment and its interaction with Nedd9 which is essential to activate the RhoA pathway cleavage furrow ingression.

Role of ABBA in neuronal migration and microcephaly

The correct formation of the cerebral cortex requires the sequential formation of cortical layers. This process is critically dependent on normal production, survival and migration of neuronal progenitors. Abnormal development of any of these processes is implicated in pathological phenotypes including microcephaly that are linked to impaired cognitive development. Within this context it is interesting that both down-regulating of Abba and the over expression of the ABBA point mutation construct results in very similar phenotypes. One plausible mechanism for these results could be explained by the disruption of the predicted local tertiary structure as indicated by the provided analysis above. This could result in the disruption of interaction with crucial proteins involved in cell cycle progression and would consist with a disruption of Nedd9 interaction and decrease RhoA activity. In this scenario, the heterozygous expression of the human R671W variant would result in a dominant negative effect on the role of ABBA in brain development linked with microcephaly and cognitive delay. Consistent with this assumption we report the clinical picture of one patient carrying the variant that displays microcephaly and developmental delay as well as two additional patients reported in Gene Matcher. Contrary to this cellular and molecular derives putative mechanism the perspective from clinical genetics is different.

From this point of view, it would be unlikely to find patients with the recurrent R671W mutation and none with a homozygous or compound heterozygous loss-of-function mutation elsewhere in the *ABBA* gene. This is against all odds, and strongly suggests a gain-of-function of the R671W mutation. Thus, further investigation is required to resolve this question in detail.

Although, previous results show that Abba is not expressed in mature neurons[20], more recent work shows that Abba can be transiently expressed in neurons during conditions of increased neuronal plasticity[13]. In the present study we deliberately focused on the role of Abba in cell radial glia proliferation but the data also indicate additional role in migration of immature neurons. This is supported by the clear accumulation of Abba-shRNA electroporated cells in the ventricular zone. Further experiments would be required to elucidate if this phenotype is truly due to intrinsic role of Abba in migrating neurons, or is provided by the disruption of the guiding radial glia. In addition, we observed a striking decrease in the total number of neuronal cells as well as length of processes in migrating cortical neurons with downregulated Abba and ABBA mutant form, but interestingly dendritic processes were increased in length and number in neurons overexpressing ABBA (Supplementary Figure 3). As it was previously described that RGP cells disorganization doesn't lead to neuronal cell death[45], these data could suggest that Abba can be involved in additional molecular mechanisms in differentiated neurons.

In conclusion, it is clear from this study that ABBA plays an important role in brain development. We present compelling evidence that a significant part of this mechanism is related to a role of ABBA during cell division of RGP. These finding is of translational

relevance as we identified a human variant with linked microcephaly and developmental disability.

Acknowledgements

We thank Drs Lauren Briere and Gabrielle Lemire for discussion about the data. We thank Biomedicum Imaging Unit (Helsinki, Finland) for their technical assistance with the time-lapse imaging of organotypic cultures. This project was supported by Eranet Neuron III program project ACROBAT, ANR project GABGANG and Academy of Finland grant 341361 to C.R., and by Fondation pour la Recherche Medicale “aide au retour en France” to A.C. Academy of Finland (317038, 319907) and Sigrid Juselius foundation to J.S. and Finnish Cultural Foundation to E.E.

Author Contributions

A.C and C.R. conceived the project and wrote the manuscript; A.C and C.R. conceived the project. A.C. designed and performed most of the experiments, analyzed and interpreted all the data, and prepared figures. A. and C.R. wrote the original draft of the manuscript. J.S. designed experiments, interpreted data, edited the manuscript. E.E: performed and analyzed experiments and edited the manuscript. H.Q performed organotypic slices culture and live imaging experiments. All authors read and approved the final manuscript.

Conflict of interest statement. None declared

References

1. Ayala, R., Shu, T. & Tsai, L.-H. Trekking across the brain: the journey of neuronal migration. *Cell* **128**, 29–43 (2007).
2. Higginbotham, H. R. & Gleeson, J. G. The centrosome in neuronal development. *Trends Neurosci.* **30**, 276–283 (2007).
3. Lambert de Rouvroit, C. & Goffinet, A. M. Neuronal migration. *Mech. Dev.* **105**, 47–56 (2001).

4. Liu, S., Xiong, X., Zhao, X., Yang, X. & Wang, H. F-BAR family proteins, emerging regulators for cell membrane dynamic changes—from structure to human diseases. *J. Hematol. Oncol.J Hematol Oncol* **8**, 47 (2015).
5. Doherty, G. J. & McMahon, H. T. Mediation, Modulation, and Consequences of Membrane-Cytoskeleton Interactions. *Annu. Rev. Biophys.* **37**, 65–95 (2008).
6. Frost, A., Unger, V. M. & De Camilli, P. The BAR Domain Superfamily: Membrane-Molding Macromolecules. *Cell* **137**, 191–196 (2009).
7. Takano, K., Takano, K., Toyooka, K. & Suetsugu, S. EFC/F-BAR proteins and the N-WASP-WIP complex induce membrane curvature-dependent actin polymerization. *EMBO J.* **27**, 2817–2828 (2008).
8. Qualmann, B., Koch, D. & Kessels, M. M. Let's go bananas: revisiting the endocytic BAR code. *EMBO J.* **30**, 3501–3515 (2011).
9. Guerrier, S. *et al.* The F-BAR domain of srGAP2 induces membrane protrusions required for neuronal migration and morphogenesis. *Cell* **138**, 990–1004 (2009).
10. Mattila, P. K. *et al.* Missing-in-metastasis and IRSp53 deform PI(4,5)P2-rich membranes by an inverse BAR domain–like mechanism. *J. Cell Biol.* **176**, 953–964 (2007).
11. Spillane, M. *et al.* The actin nucleating Arp2/3 complex contributes to the formation of axonal filopodia and branches through the regulation of actin patch precursors to filopodia. *Dev. Neurobiol.* **71**, 747–758 (2011).
12. Saarikangas, J. *et al.* MIM-Induced Membrane Bending Promotes Dendritic Spine Initiation. *Dev. Cell* **33**, 644–659 (2015).
13. Chatzi, C. *et al.* Exercise-induced enhancement of synaptic function triggered by the inverse BAR protein, Mtss1L. *eLife* **8**, e45920 (2019).
14. Wilson, N. K. A. *et al.* A Novel Microduplication in the Neurodevelopmental Gene SRGAP3 That Segregates with Psychotic Illness in the Family of a COS Proband. *Case Rep. Genet.* **2011**, 585893 (2011).

15. Carlson, B. R. *et al.* WRP/srGAP3 facilitates the initiation of spine development by an inverse F-BAR domain, and its loss impairs long-term memory. *J. Neurosci. Off. J. Soc. Neurosci.* **31**, 2447–2460 (2011).
16. Endris, V. *et al.* The novel Rho-GTPase activating gene MEGAP/ srGAP3 has a putative role in severe mental retardation. *Proc. Natl. Acad. Sci. U. S. A.* **99**, 11754–11759 (2002).
17. Waltereit, R. *et al.* Srgap3^{-}/$^{-}$ mice present a neurodevelopmental disorder with schizophrenia-related intermediate phenotypes. *FASEB J. Off. Publ. Fed. Am. Soc. Exp. Biol.* **26**, 4418–4428 (2012).
18. Saitsu, H. *et al.* Early infantile epileptic encephalopathy associated with the disrupted gene encoding Slit-Robo Rho GTPase activating protein 2 (SRGAP2). *Am. J. Med. Genet. A.* **158A**, 199–205 (2012).
19. Alazami, A. M. *et al.* Accelerating Novel Candidate Gene Discovery in Neurogenetic Disorders via Whole-Exome Sequencing of Prescreened Multiplex Consanguineous Families. *Cell Rep.* **10**, 148–161 (2015).
20. Saarikangas, J. *et al.* ABBA regulates plasma-membrane and actin dynamics to promote radial glia extension. *J. Cell Sci.* **121**, 1444–1454 (2008).
21. Dadke, D., Jarnik, M., Pugacheva, E. N., Singh, M. K. & Golemis, E. A. Deregulation of HEF1 impairs M-phase progression by disrupting the RhoA activation cycle. *Mol. Biol. Cell* **17**, 1204–1217 (2006).
22. Yu, J.-Y., DeRuiter, S. L. & Turner, D. L. RNA interference by expression of short-interfering RNAs and hairpin RNAs in mammalian cells. *Proc. Natl. Acad. Sci. U. S. A.* **99**, 6047–6052 (2002).
23. Adzhubei, I. A. *et al.* A method and server for predicting damaging missense mutations. *Nat. Methods* **7**, 248–249 (2010).

24. Sobreira, N., Schiettecatte, F., Valle, D. & Hamosh, A. GeneMatcher: a matching tool for connecting investigators with an interest in the same gene. *Hum. Mutat.* **36**, 928–930 (2015).
25. van Rheenen, J., Langeslag, M. & Jalink, K. Correcting confocal acquisition to optimize imaging of fluorescence resonance energy transfer by sensitized emission. *Biophys. J.* **86**, 2517–2529 (2004).
26. Saito, T. & Nakatsuji, N. Efficient gene transfer into the embryonic mouse brain using in vivo electroporation. *Dev. Biol.* **240**, 237–246 (2001).
27. Tabata, H. & Nakajima, K. Efficient in utero gene transfer system to the developing mouse brain using electroporation: visualization of neuronal migration in the developing cortex. *Neuroscience* **103**, 865–872 (2001).
28. Wiegreffe, C., Feldmann, S., Gaessler, S. & Britsch, S. Time-lapse Confocal Imaging of Migrating Neurons in Organotypic Slice Culture of Embryonic Mouse Brain Using In Utero Electroporation. *J. Vis. Exp. JoVE* (2017) doi:10.3791/55886.
29. Kosodo, Y. Interkinetic nuclear migration: beyond a hallmark of neurogenesis. *Cell. Mol. Life Sci.* **69**, 2727–2738 (2012).
30. Spear, P. C. & Erickson, C. A. Apical movement during interkinetic nuclear migration is a two-step process. *Dev. Biol.* **370**, 33–41 (2012).
31. Tsai, J.-W., Lian, W.-N., Kemal, S., Kriegstein, A. R. & Vallee, R. B. Kinesin 3 and cytoplasmic dynein mediate interkinetic nuclear migration in neural stem cells. *Nat. Neurosci.* **13**, 1463–1471 (2010).
32. Hu, D. J.-K. *et al.* Dynein recruitment to nuclear pores activates apical nuclear migration and mitotic entry in brain progenitor cells. *Cell* **154**, 1300–1313 (2013).
33. Carabalona, A., Hu, D. J.-K. & Vallee, R. B. KIF1A inhibition immortalizes brain stem cells but blocks BDNF-mediated neuronal migration. *Nat. Neurosci.* **19**, 253–262 (2016).
34. Miller, A. L. The contractile ring. *Curr. Biol. CB* **21**, R976-978 (2011).

35. Zhang, S. & Wu, L. Roles of neural precursor cell expressed, developmentally downregulated 9 in tumor-associated cellular processes (Review). *Mol. Med. Rep.* **12**, 6415–6421 (2015).
36. Zhong, J. *et al.* NEDD9 stabilizes focal adhesions, increases binding to the extra-cellular matrix and differentially effects 2D versus 3D cell migration. *PloS One* **7**, e35058 (2012).
37. Singh, M., Cowell, L., Seo, S., O'Neill, G. & Golemis, E. Molecular basis for HEF1/NEDD9/Cas-L action as a multifunctional co-ordinator of invasion, apoptosis and cell cycle. *Cell Biochem. Biophys.* **48**, 54–72 (2007).
38. Jarin, Z. *et al.* Unusual Organization of I-BAR Proteins on Tubular and Vesicular Membranes. *Biophys. J.* **117**, 553–562 (2019).
39. Glotzer, M. Animal cell cytokinesis. *Annu. Rev. Cell Dev. Biol.* **17**, 351–386 (2001).
40. Klingler, E., Francis, F., Jabaudon, D. & Cappello, S. Mapping the molecular and cellular complexity of cortical malformations. *Science* **371**, eaba4517 (2021).
41. Jumper, J. *et al.* Highly accurate protein structure prediction with AlphaFold. *Nature* **596**, 583–589 (2021).
42. Field, S. J. *et al.* PtdIns(4,5)P2 functions at the cleavage furrow during cytokinesis. *Curr. Biol. CB* **15**, 1407–1412 (2005).
43. Normand, G. & King, R. W. Understanding cytokinesis failure. *Adv. Exp. Med. Biol.* **676**, 27–55 (2010).
44. Zhang, S. & Wu, L. Roles of neural precursor cell expressed, developmentally downregulated 9 in tumor-associated cellular processes (Review). *Mol. Med. Rep.* **12**, 6415–6421 (2015).
45. Carabalona, A. *et al.* A glial origin for periventricular nodular heterotopia caused by impaired expression of Filamin-A. *Hum. Mol. Genet.* **21**, 1004–1017 (2012).

Figures Legends

Figure 1. *In utero* knockdown of Abba expression is linked to radial glial disruption and alters neuronal migration.
A. Representative coronal sections of E16-E18 mice brains electroporated at E14 with either scramble or Abba-shRNA3 and immunostained for vimentin (in blue). In Abba-shRNA3 brain sections, vimentin staining revealed a marked disruption of radial glial apical fibers. **B.** Representative neocortical coronal sections showing migration of transfected cells 3 days after electroporation at E14 with either scramble or Abba-shRNA3. **C.** Quantification of RFP-positive cell distribution in the cortex at E17 (VZ/SVZ: scramble 24.33±2.13%, Abba-shRNA3 63.71±1.03%; IZ: scramble 39.80±2.22%, Abba-shRNA3 29.71±0.85%; CP: scramble 35.86±1.73%; Abba-shRNA3 6.58±0.53%; n=9 scramble and 8 Abba-shRNA3; (VZ/SVZ: p=<0.0001: IZ: p=0.0002; CP: p=<0.0001) showing a significant increase of Abba knockdown cells in SVZ/lower IZ. **D.** Higher magnifications of regions indicated by a square in C. **E.** Total number of RFP positive cells in mouse neocortex at E17 (scramble 969.2±109.0%; Abba-shRNA3 311.3±28.61%; n=9 scramble and 8 Abba-shRNA3) showing a striking reduction of RFP positive cells in Abba knockdown electroporated brains. Error bars represent mean ± s.d. **P < 0.002, ***P < 0.001, Scale bars 100μm (A). **F.** Quantification of radial glial progenitor cells at the VZ (scramble 126.50±13.36%, Abba-shRNA3 65.14±9.91%). mean ±SD. VZ: ventricular Zone, IZ: Intermediate Zone, CP: Cortical Plate. Error bars represent mean ± s.d. **P < 0.002. Scale bars 100μm (A), 50μm (B).

Figure 2. Abba down regulation induced inhibition of basal nuclear migration in RGP cells blocks cell cycle progression. A. Quantification of the nuclear distance from the VS for RGP cells after electroporation of scrambled or Abba-shRNA3. Nuclear distribution of RFP RGP cells was significantly altered after electroporation of Abba-shRNA3 (0–10: scramble, 30.20 ± 1.21%; Abba-shRNA3, 38.34 ± 0.89%; 10–20: scramble, 34.35 ± 0,69%; Abba-shRNA3, 22.80 ± 1.03%; 20–30: scramble, 23.42 ± 1.00%; Abba-shRNA3, 17.00 ± 1.10%; >30: scramble, 12.04 ± 1.27%; Abba-shRNA3, 21.85 ± 0.74%; (0–10: P = 0,000156; 10-20: P=<0.000001; 20-30:P= 0,001030; >30:P= 0,000023). **B-C.** E14 mice brains were subjected to *in utero* electroporation with either scramble or Abba- shRNA3. Brains were then fixed at E17 and stained with the RGP cell marker Pax6. We observe an important decrease of Pax6 RGP cells expressing Abba RNAi (scramble, 31.87 ± 0.57%; Abba-shRNA3, 21.08 ± 0.63%; n = 8 scramble; 5 Abba-shRNA3). **D-G.** E14 mice brains were subjected to *in utero* electroporation with either scramble or Abba-shRNA3. Brains were then fixed at E17 and stained with the cell cycle marker KI67 (D)and PH3 (F). We observe a striking decrease in the percent of cycling (E: Ki67; scramble, 46.54 ± 0.79%, n=7; Abba-shRNA3, 23.71 ± 1.37%, n=5 Abba-shRNA3)) and but not in mitotic (PH3; scramble, 4.50 ± 0.17%; Abba-shRNA3, 4.25 ± 0.65%) cells with low expression of Abba. Error bars represent mean ± s.d. **P < 0.002, ***P < 0.001. Scale bar represents 20 μm.

Figure 3. Abba down regulation blocks cytokinesis
A. Cellular distribution of Abba in C6 cells during cell division. Upper panel shows two example immunofluorescent microscopy images of Abba (red). Left most figure shows the projection images at the cross line of the image**.** Mid and lower panels show the distribution of Abba at different cell division stages in relation to β-tubulin (green) aggregation **B.** Immunofluorescence microscopy images from C6 cells 72 hours after transfection with Abba-shRNA3 shows an absence of Abba expression at cytokinesis. **C.** Brain slices prepared following *in utero* electroporation with Abba-shRNA3 or scramble were cultured at E17 and monitored by live imaging for 15–20 h. Time lapse duration shown (in h:min) was varied as needed to include major INM events. Scramble RGP cell underwent one mitosis at the ventricular surface of the brain slice (1:50; 2:20), we can observe two cells at timepoint 3:00 (arrows) and the presence of basal fibers (arrowheads). Nucleus of Abba knockdown RGP (arrow) initially underwent apical INM and divided (8:30) and remained at the ventricular surface for at least 7h, suggesting that the absence of Abba prevents cells from leaving mitosis **D**. Quantification of the total number of RFP positive cells in the neocortex illustrating the impact of cytokinesis block on cell survival. We observed a lower total number of cells

4 days after transfection with Abba-shRNA3 compared with control scramble (scramble 380,3± 48,16%; n=12, Abba-shRNA3 155,8± 22,32%; p= <0.0001; n=12). **E.** Error bars represent mean ± s.d. *P < 0.03, **P < 0.002, ***P < 0.001. Scale bar represents 50 μm (A), 20 μm (D).

Figure 4. Role of Abba-Nedd9 complex in RGP cells division

A. Good and high confidence interactions detected in yeast two-hybrid screen performed in mouse brain embryo library using full length mouse Abba as a bait. **B.** Schematic representation of the Abba and Nedd9 proteins. **C.** C6 cells expressing GFP–Nedd9 were subjected to a direct pulldown assay with endogenous Abba. GFP–Nedd9, but not GFP, co-immunoprecipitated with endogenous Abba, indicating the specificity of the interaction. **D**. immunocytochemistry on C6 cells 72 hours after transfection with Abba-shRNA3 shows that lack of Abba did not decrease Nedd9 expression (green) but rather its localization. Scale bars 20μm. **E.** Representative coronal sections of E17 mice brains transfected at E14 with Nedd9-shRNA and immunostained for vimentin (in blue). Vimentin staining revealed a marked disruption of radial glial apical fibers. **F.** Quantification of RFP-positive cell distribution in the cortex at E17 (VZ/SVZ: scramble 25 ± 2.30%, Nedd9-shRNA 46.92±2.78%; IZ: scramble 38.94±2.32%, Nedd9-shRNA 37.37±2.96%; CP: scramble 36.06±1.95%; Nedd9-shRNA 15.71±2.25%; n=8 scramble and 7 Nedd9-shRNA; (VZ/SVZ: p=<0.0001: IZ: p=0.0002; CP: p=<0.0001) showing a significant increase of Nedd9 knockdown cells in SVZ/lower IZ.

Figure 5. Abba downregulation decreases RhoA activity.

A. Confocal images of C6 cells 72 hours after transfection with Raichu-RhoA either with Abba-shRNA3 or scramble. The efficacy of Raichu-RhoA was tested using Calpeptin, a RhoA activator. **B.** Quantification of FRET density (Raichu-RhoA activity) showed a decreased of Raichu-RhoA activity in C6 cells transfected with Abba-shRNA3 as compared to the ones transfected with the scramble (scramble 12.03±0.34; n=81, Abba-shRNA3 7.93±0.34; n=27; p<0.0001; Raichu-RhoA without Calpeptin: 12.15±0.36 n=52; Raichu-RhoA + Calpeptin: 14.48±0.61 n=33; p=0.002). Error bars represent mean ± s.d. **P < 0.002, ***P < 0.001. Scale bars 100μm (**A**).

Figure 6. Effect of ABBA R671W human mutation on neuronal migration and mitosis

A. ABBA is composed of an N-terminal BAR domain, a serine-rich region, three proline-rich motifs and a C-terminal WH2 domain. **B.** Evolutionary conservation analysis revealed that the Arg671 site is conserved from zebrafish to humans. **C.** Representative brain imaging features of one patient carrying ABBA R671W mutation. **D.** 3D structure of ABBA denoting the position of Arginine 571. Lower panel show the high probability of disruption of the a-helix conformation by a Arginine to Tryptophane mutation. **E.** Coronal sections of E17 mice brains electroporated at E14 with cDNAs encoding the human wild-type, ABBA-FL, or the human mutant form of ABBA, ABBA-R671W. Expression of ABBA-R671W results in a defect in neuronal migration as indicated by the accumulation of neurons in the SVZ/lower IZ as well as a disorganization of the radial glial cell fibers using vimentin staining. **F.** Quantification of cell distribution in the cortex at E17 (VZ/SVZ: ABBA-FL 18.67±1.44%, ABBA-R671W 39.77±2.73%; IZ: ABBA-FL 53.07±2.37%, ABBA-R671W 43.40±1.40%; CP: ABBA-FL 28.25±1.25%, ABBA-R671W 16.8±2.03%; n=6 ABBA-FL and X ABBA-R671W) showing a significant increase of mutant cells in SVZ/lower IZ. **G.** Quantification of the distance of RGP nuclei from the ventricular surface (VS) at E17 (0–10: ABBA-FL 32.56±2.58%, ABBA-R671W 50,04±2.04%; 10–20: ABBA-FL 34.37±0,59%, ABBA-R671W 25.76±1.97%; 20–30: ABBA-FL 22.08±1.59%, ABBA-R671W 16.12±2.12%; >30: ABBA-FL 10.99±1.52%, ABBA-R671W 7.71±1.38%; n=8 ABBA-FL and 6 ABBA-R671W), revealing accumulation at this site for the mutant, but not wild-type ABBA. (VZ/SVZ: p=0.000001: IZ: p=0.0014; CP: p=0.0003; 0–10: p=0.0002; 10–20: p=0.0005; 20–30: p=0.040; >30: p=0.150); mean ± SD. **H.** Brains were then fixed at E17 and stained with the mitotic marker Phopho-Histone3 (PH3). **I.** The percentage of PH3-positive nuclei located at the ventricular surface (VS) did not differ in RGP cells expressing ABBA-R671W (ABBA-FL, 4.50±0.17%, n=9; ABBA-R671W, 4.71±0.88%, n=5, P=0.761;). Error bars represent mean ± s.d. **P < 0.01, ***P < 0.001. VZ: ventricular Zone, IZ: Intermediate Zone, CP: Cortical Plate. Scale bars 100μm (A), 15μm (D).

Table 1. Summary of clinical and imaging phenotypes associated with mutations in ABBA

Supplemental figure 1. Alteration of Abba expression by RNAi
Schematic diagram showing the position of small-hairpin RNAs targeting the coding sequence (CDShp) and the 3′UTR of Abba mRNA. **B.** Knockdown of endogenous Abba mRNA expression in rat C6 glioma cells was measured by qPCR 72 h after transfection with CDShp or 3UTRhp. We observed a reduction of Abba mRNA expression by 70% with Abba-shRNA3 compared with corresponding ineffective shRNAs (Abba-shRNA1 and Abba-shRNA2) or the control scramble. Rpl13a was used for normalization. **C.** Western blot analysis revealed that Abba protein levels, 72 h after transfection, were much lower in cells transfected with Abba-shRNA3 compared with those transfected with scramble and with non-transfected (control) cells. α-Tubulin was used for normalization. **D.** We observed a reduction of Abba expression in Rat C6 glioma cells, 72h after transfection with Abba-shRNA3 compared with cells transfected with scramble. Error bars represent mean ± s.d. **P < 0.02, ***P < 0.001. Scale bars: 20 µm (D).

Supplemental figure 2. ¨Nedd9 shRNA efficiency test in C6 cells and effect on nr of PH3 positive cell *in vivo*.
Quantification of Nedd9 mRNA expression in C6 cell after 72h transfection with four different shRNA constructs. Sh3 most efficiently decreased Nedd9 expression. Mim was used as a control for specificity of the shRNA knock - down. **B.** Nedd9- shRNA electroporated brains were stained with the late G2/M phases marker Phopho-Histone3 (PH3). **C.** The percentage of PH3-positive nuclei located at the ventricular surface (VS) greatly increased in RGP cells expressing Nedd9-shRNA (scramble, 4.50±0.18%, n=9; Nedd9-shRNA, 5.07±0.35%, n=6, P=0,1135;). Error bars represent mean ± s.d. **P < 0.002, ***P < 0.001. VZ: ventricular Zone, IZ: Intermediate Zone, CP: Cortical Plate. Scale bars 100µm (A), 20µm (D).

Movie 1: symmetric division

Related to Figure 3C, top panel. E14 mouse embryonic brain was electroporated with vectors expressing Abba shRNA and RFP. Brain was sectioned at E17 and imaged every 15 minutes. Nucleus of RGP cell apically migrated to the ventricular surface and underwent symmetric division.

Movie 2: absence of division in Abba depleted progenitor cells

Related to Figure 3C, bottom panel. E14 mouse embryonic brain was electroporated with vectors expressing Abba shRNA and RFP. Brain was sectioned at E17 and imaged every 15 minutes. Nucleus of RGP cell apically migrated to the apical surface and remains block at the ventricular surface for hours without being able to enter mitosis.

Figure 1

A

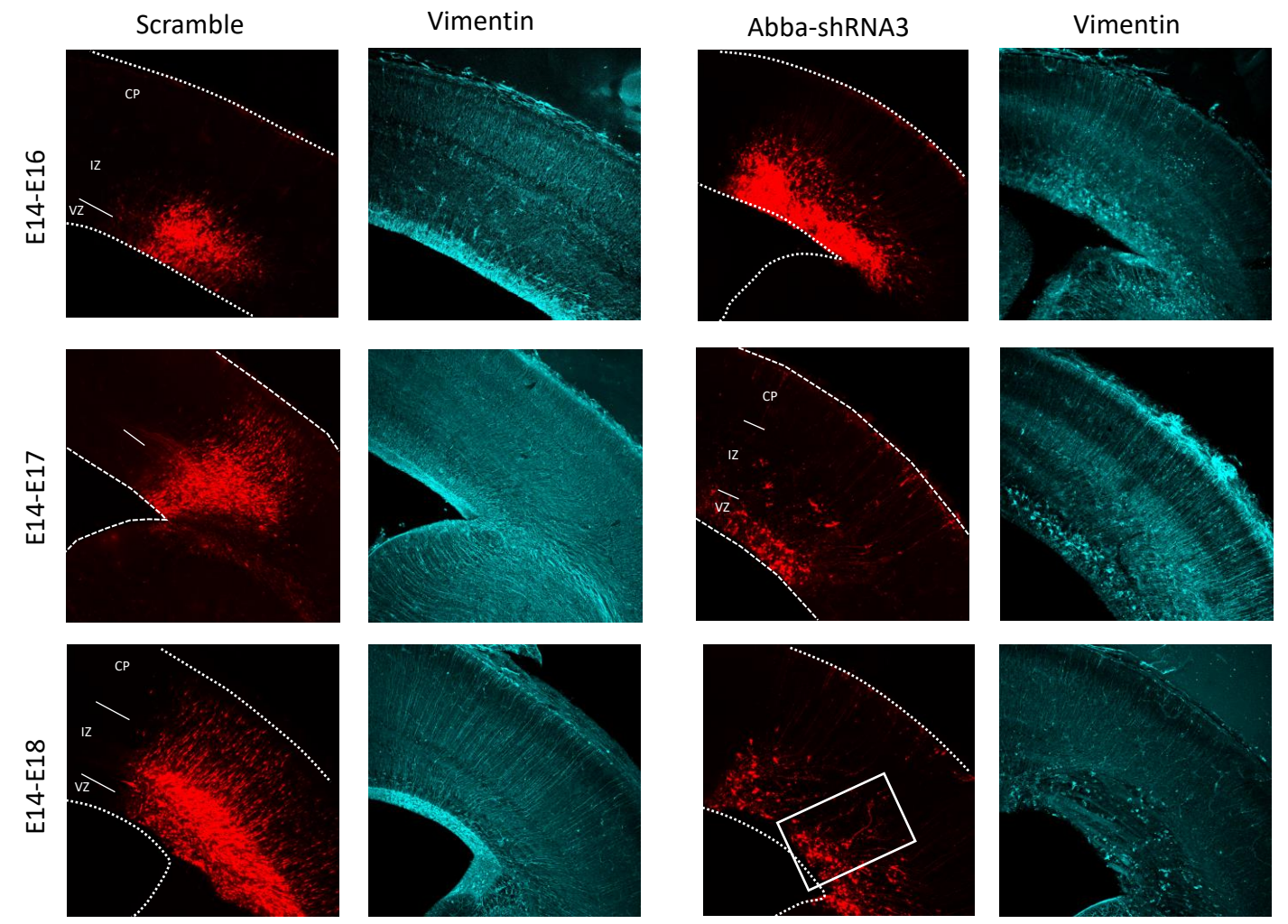

B

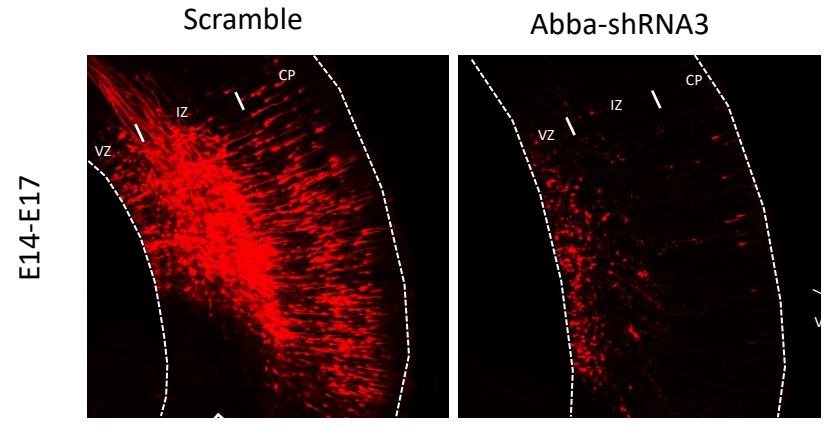

C

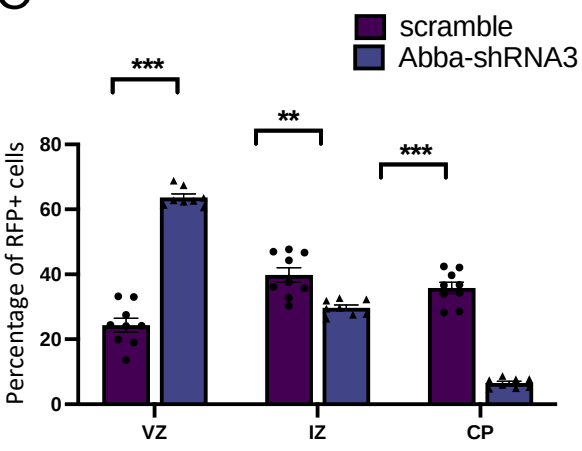

D

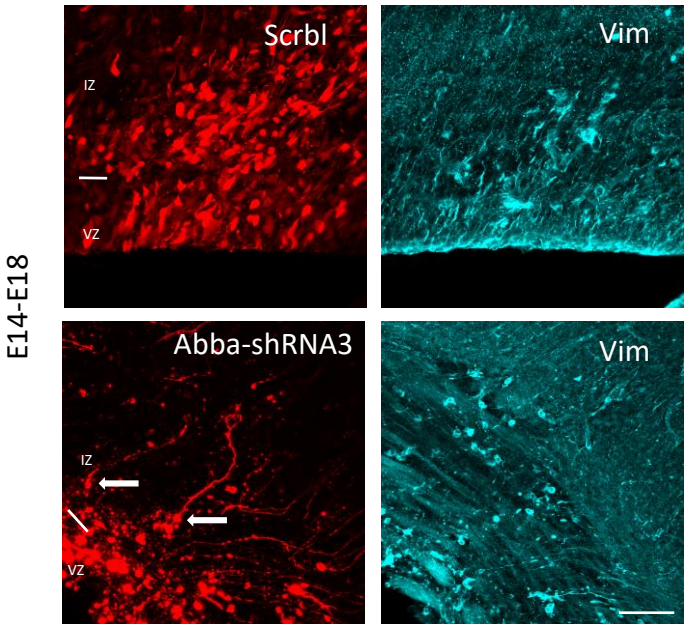

E

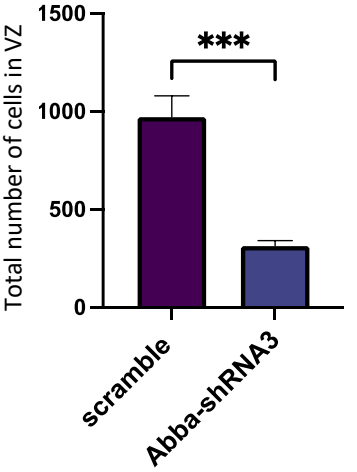

F

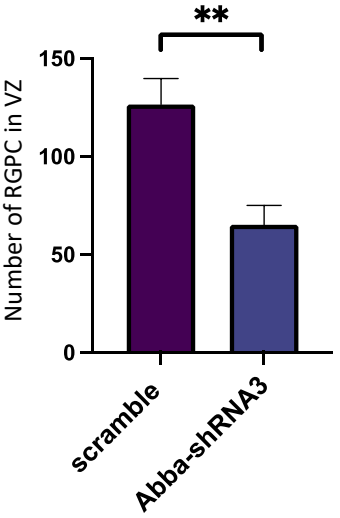

Figure 2

A

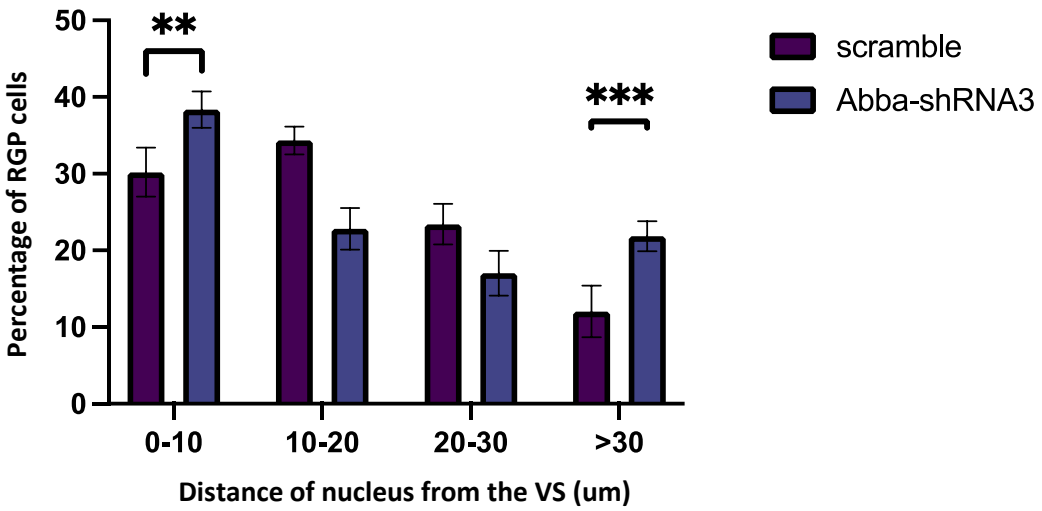

B

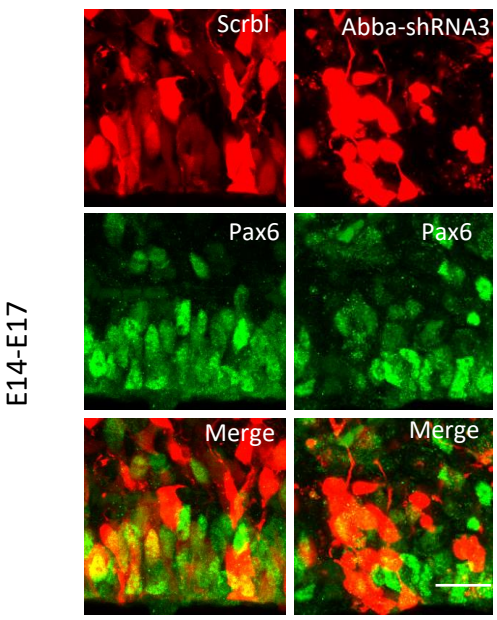

C

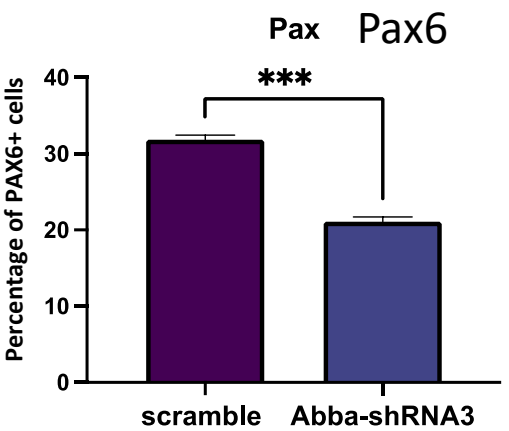

D

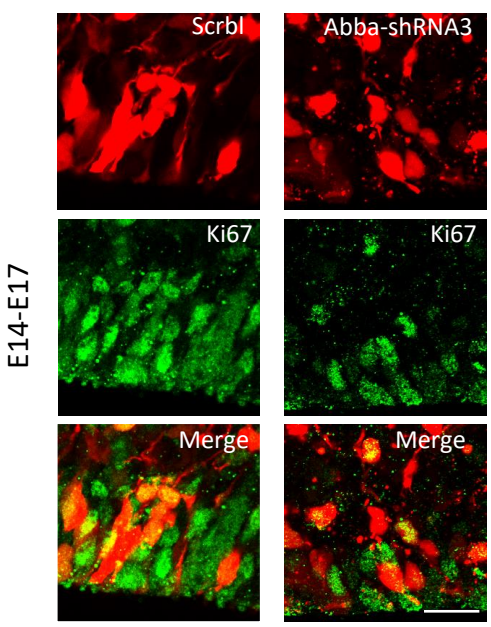

F

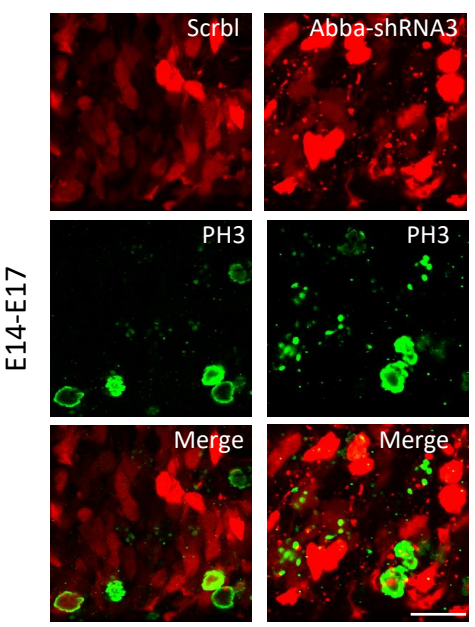

E

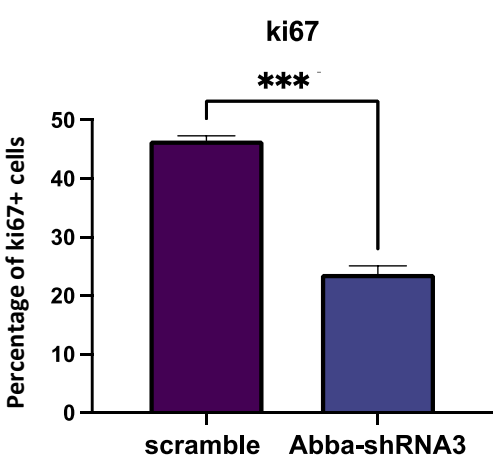

G

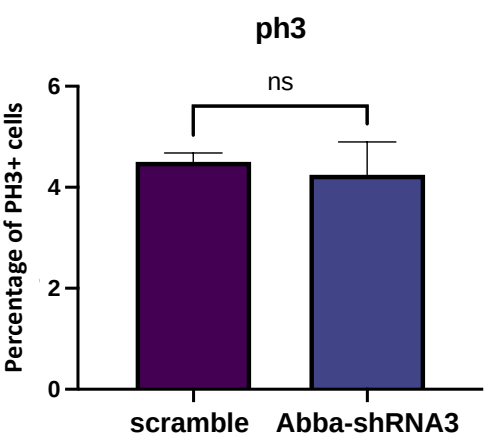

Figure 3

A

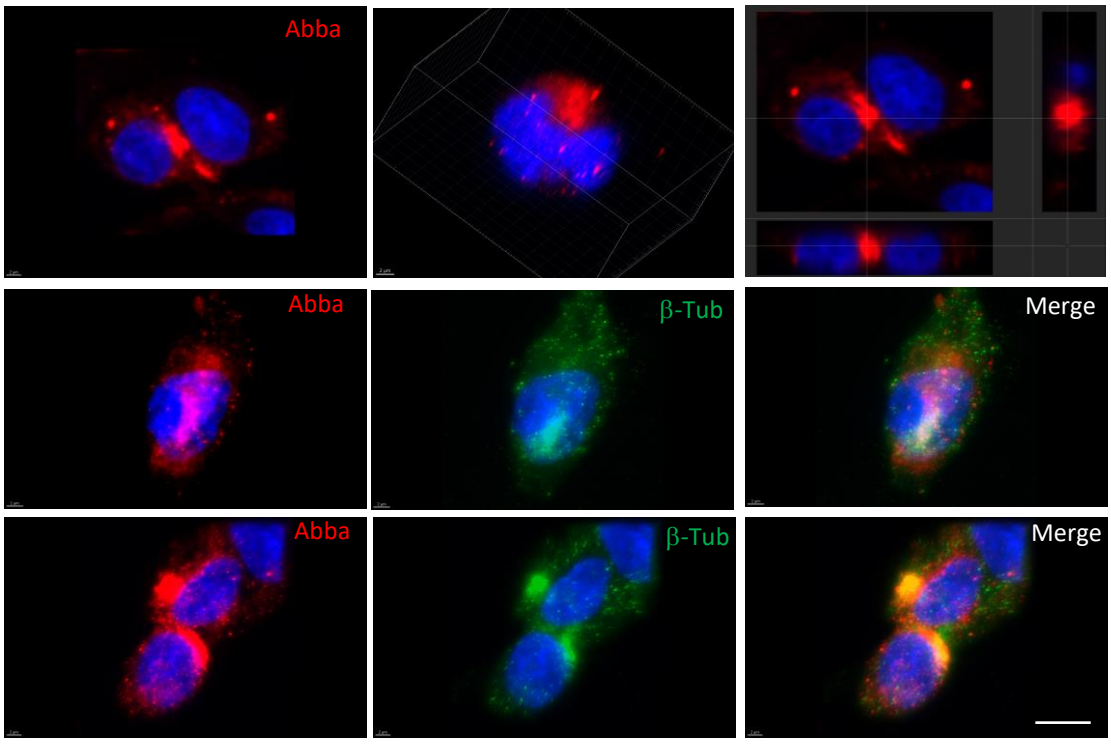

B

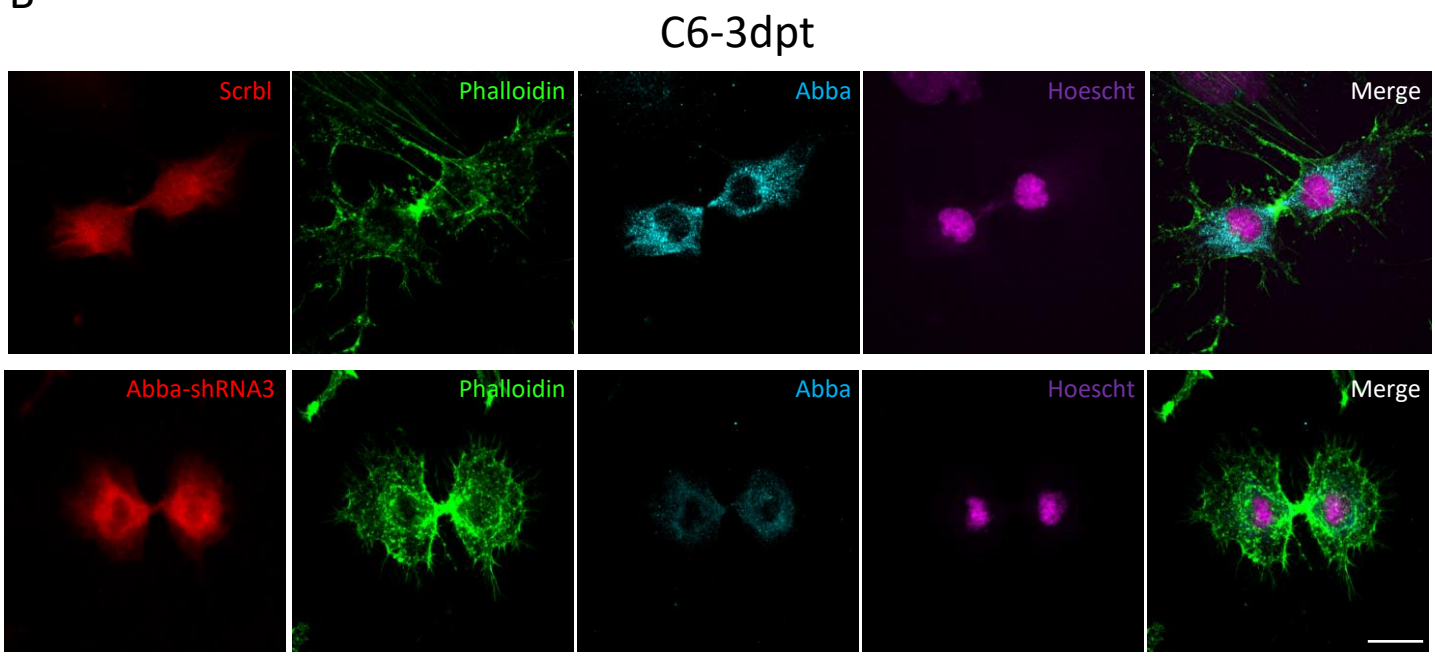

C

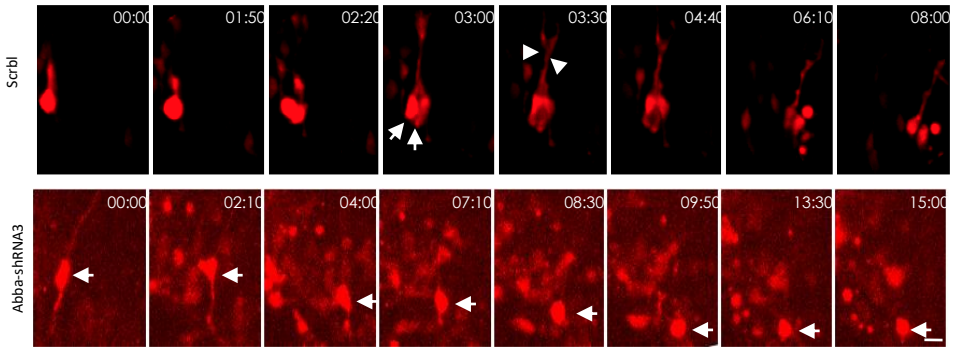

D

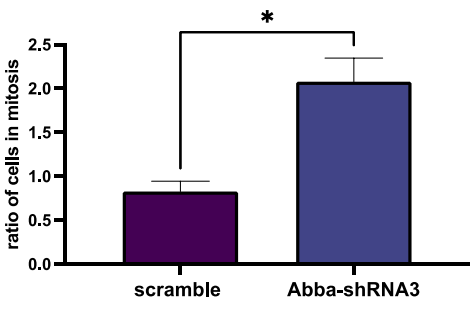

E

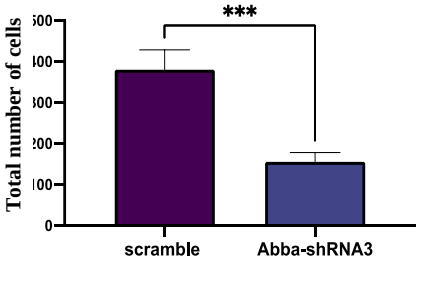

Figure 4

A

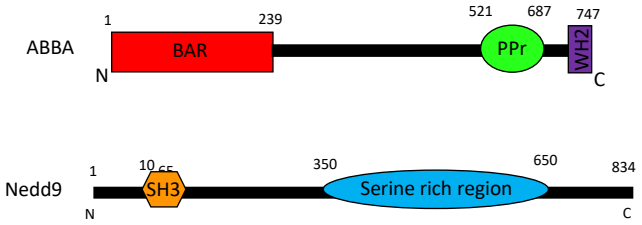

B

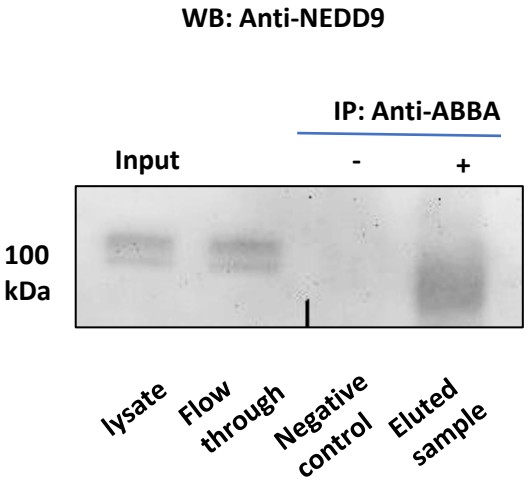

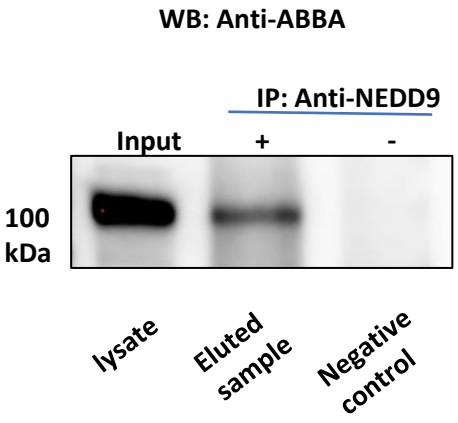

C

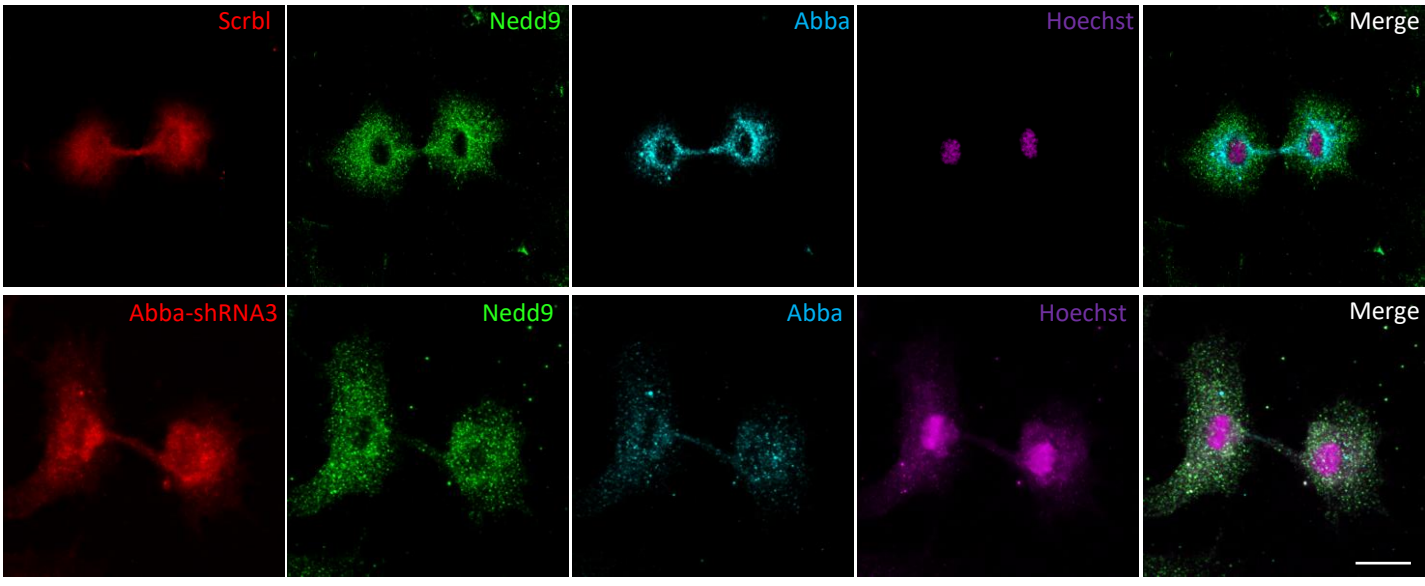

D

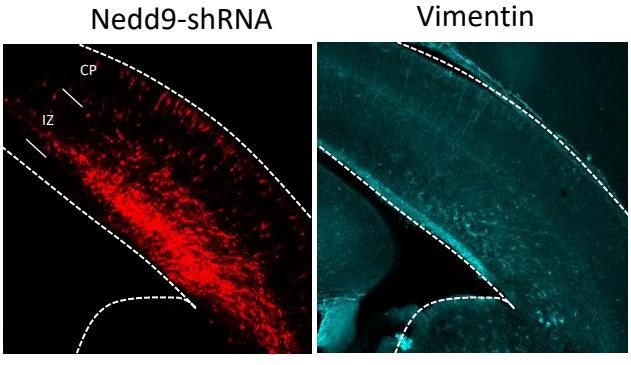

E

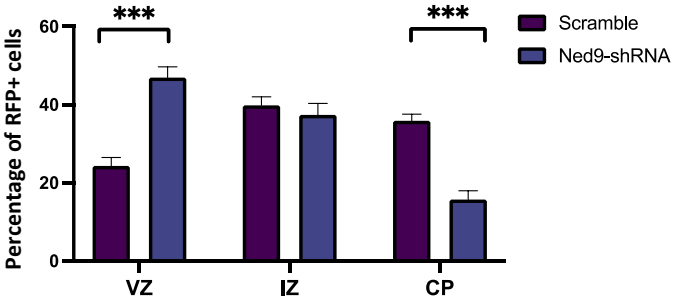

Figure 5

A

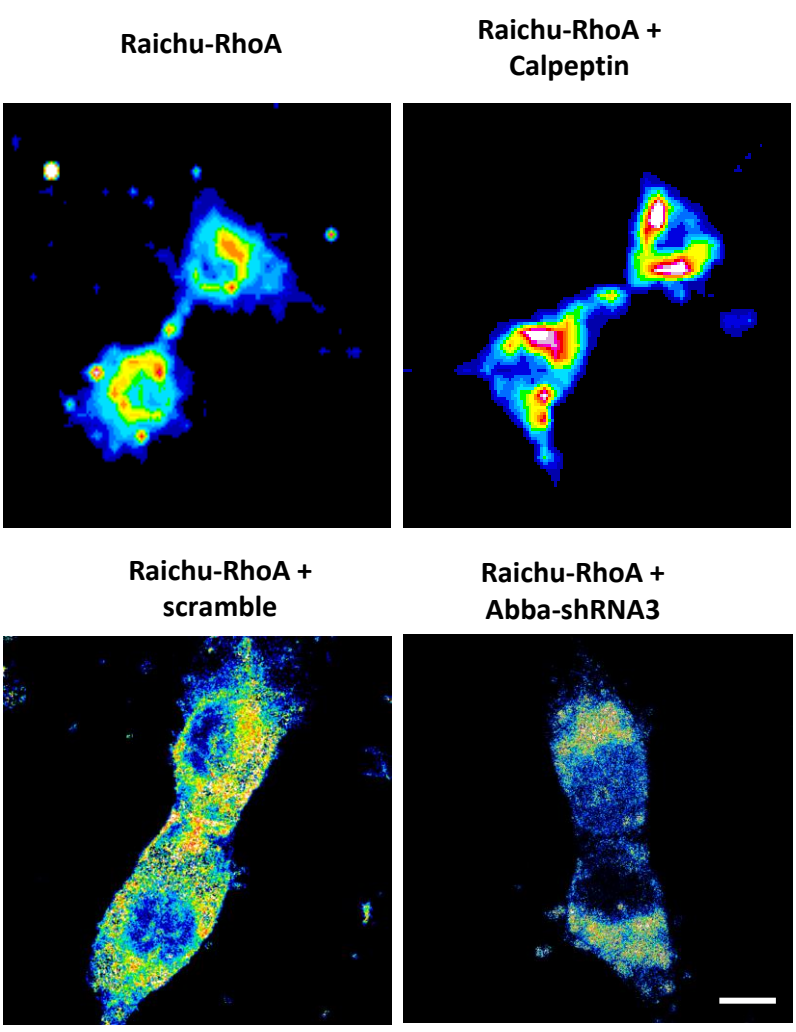
Raichu-RhoA
Raichu-RhoA + Calpeptin
Raichu-RhoA + scramble
Raichu-RhoA + Abba-shRNA3

B

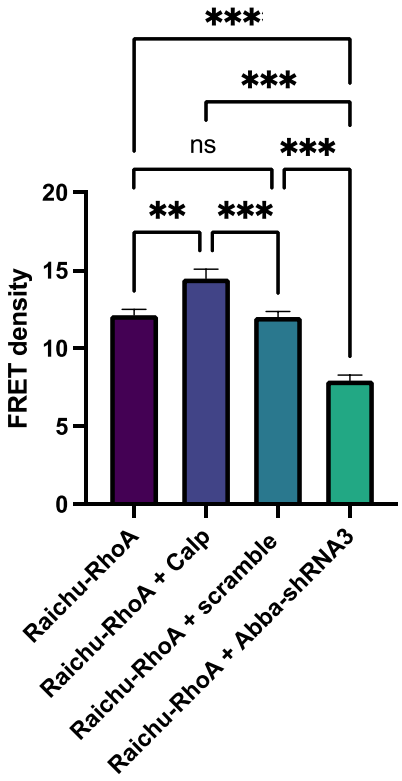
***
***
ns
***
**
***
FRET density
20
15
10
5
0
Raichu-RhoA
Raichu-RhoA + Calp
Raichu-RhoA + scramble
Raichu-RhoA + Abba-shRNA3

Figure 6

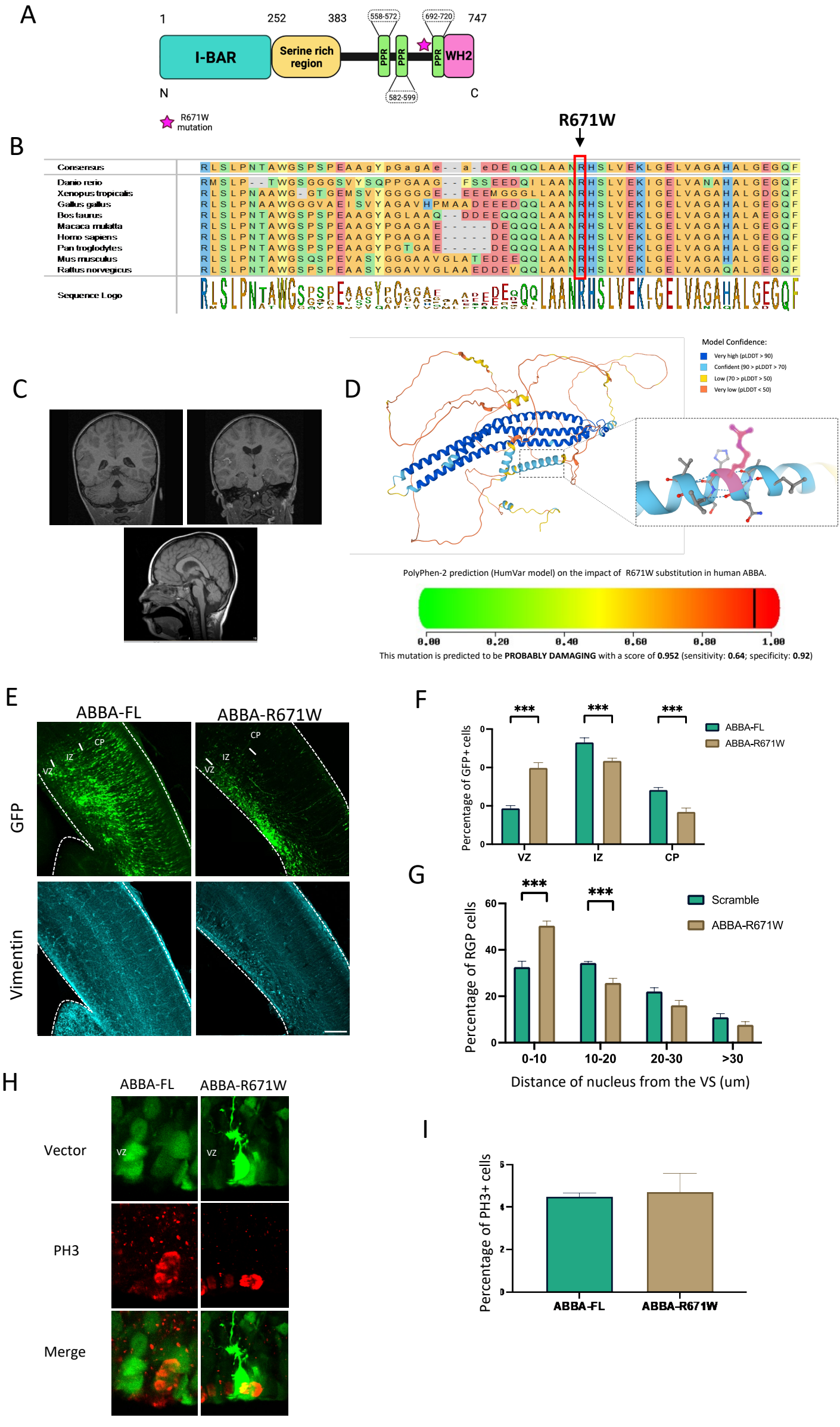
A
1
252
383
558-572
692-720
747
I-BAR
Serine rich region
PPR
PPR
PPR
WH2
582-599
N
C
R671W mutation
B
R671W
Consensus
Danio rerio
Xenopus tropicalis
Gallus gallus
Bos taurus
Macaca mulatta
Homo sapiens
Pan troglodytes
Mus musculus
Rattus norvegicus
Sequence Logo
C
D
Model Confidence:
Very high (pLDDT > 90)
Confident (90 > pLDDT > 70)
Low (70 > pLDDT > 50)
Very low (pLDDT < 50)
PolyPhen-2 prediction (HumVar model) on the impact of R671W substitution in human ABBA.
0.00
0.20
0.40
0.60
0.80
1.00
This mutation is predicted to be PROBABLY DAMAGING with a score of 0.952 (sensitivity: 0.64; specificity: 0.92)
E
ABBA-FL
ABBA-R671W
GFP
Vimentin
VZ
IZ
CP
F
Percentage of GFP+ cells
ABBA-FL
ABBA-R671W
VZ
IZ
CP
G
Percentage of RGP cells
Scramble
ABBA-R671W
0-10
10-20
20-30
>30
Distance of nucleus from the VS (um)
H
ABBA-FL
ABBA-R671W
Vector
PH3
Merge
I
Percentage of PH3+ cells
ABBA-FL
ABBA-R671W